Proceedings of the Fifth IASTED International Conference
VISUALIZATION, IMAGING, AND IMAGE PROCESSING
September 7-9, 2005, Benidorm, Spain

A PRACTICAL WAY TO INITIALIZE CAMERA PARAMETERS USING THE ABSOLUTE CONIC

Tomislav Pribanic*, Peter Sturm**, Mario Cifrek*
*Faculty of electrical engineering and computing, University of Zagreb, Unska 3, HR-10000**
*INRIA Rhône-Alpes, 655, avenue de l'Europe, 38330 Montbonnot St Martin, France***
tomislav.pribanic@fer.hr, peter.sturm@inria.fr, mario.cifrek@fer.hr

ABSTRACT
A very common and effective approach for 3D reconstruction is a camera based system where 3D information is extracted from images. Different systems involve different camera calibration methods/tools. Characteristically for many systems is to calibrate the cameras using a single wand of known length. As integral part of the calibration procedure, initial camera parameters are commonly computed by putting and imaging two or three orthogonal wands inside the working volume. This is usually followed by the second step: sweeping the working volume with a single wand of known length. This paper presents two alternative ways of initializing camera parameters using essentially the same calibration tools (orthogonal wands), however by sweeping the volume with an orthogonal pair or triad of wands instead of a single one. The proposed methods exploit the orthogonality of the used wands and familiar linear constraints to calculate the image of the so-called absolute conic (IAC). Extracted internal parameters values from IAC are closer to the refined ones, assuring faster and safer convergence. Even without refinement, sometimes not necessary, reconstruction results using our initial sets are better than using commonly obtained initial values. Besides, the entire calibration procedure is shortened since the usual two calibration steps become one.

KEY WORDS
camera calibration, 3D reconstruction, absolute conic

1. Introduction

3D reconstruction of points in space is a task present in a variety of areas and applications: entertainment, animation, industrial design, sports/medicine etc. Different applications contributed to parallel developments of a variety of principles (and instrumentations) to obtained 3D information [1]. One of the many areas where 3D reconstruction is highly desired is the field of human motion analysis [2]. A very common and effective approach for that particular purpose uses camera based systems. The image created by a camera represents a two-dimensional projection of a three-dimensional object. Two such images are sufficient to yield 3D coordinates by the means of photogrammetric reconstruction [3]. Prior to the reconstruction of the unknown object points, a camera calibration procedure takes place.

The projection of a point from 3D space to the 2D camera image sensor plane is described by a camera model and the parameters of that model. Calibration is a process during which particular parameters are determined [4]. Over the course of years different methods/tools evolved in order to make calibration as simple as possible and at the same time satisfying a high degree of reconstruction accuracy. Essentially, we need to provide images whose known scene geometry can be used to calibrate camera. An easy way to do this is to build and image a special calibration object of some kind. Traditionally, data for calibration were provided by some form of 3D calibration cage. Such an approach, apart from apparent advantages of being rather accurate and reliable, has many disadvantages that nowadays are less and less acceptable. For instance, accurate fabrication, manipulation and storage of 3D cages very often asks for considerable amounts of money, patience (sometimes even with no guarantee that calibration will be successful after all) and space, respectively. All those conditions are quite relaxed if we decide to calibrate cameras using calibration planes, i.e. 2D calibration tools [5], [6]. Taking one more step in simplifying things is to use 1D calibration objects [7]. There is an ongoing tendency to make calibration methods as simple as possible and using as little data as possible. These approaches heavily rely on (hopefully) readily available scene constraints and/or assumptions about camera parameters (spatial configurations) [8], [9], [10], [11]. The ultimate goal of auto-calibration (calibration without any specific calibration object) is theoretically feasible, but often inapplicable in practice due to unrealistic assumptions about camera parameters and/or degenerate camera configuration [12], which are typical for a certain applications.

Presently a lot of commercially available systems are offering camera calibration using simply wand(s) of known length(s), for example [13]. A typical procedure of such 3D reconstruction systems consists of two steps. The first step requires to place and image two or three orthogonal wands. The origin and orientation of these wands actually determine the spatial coordinate system in

accordance with user needs. Additionally each wand has a certain number of markers, whose relative positions are known, so that the correspondence between 3D space and camera image planes can be readily established and used to initialize camera parameters. Due to the existence of various sources of errors or noise, primarily those caused by lens imperfection and non linear distortion, these initial estimates of camera parameters are only rough approximations [14]. The task of the second calibration step is to refine these initial cameras parameters by waving with a wand of known length (so called wand dance) throughout the desired calibration volume.

The aim of this paper is to use commonly present calibration tools (orthogonal wands with attached markers) and to investigate the applicability of alternative scene constraints that would allow a better parameter initialization, i.e. closer to the true parameter values and/or providing better reconstruction accuracy right from the start. Providing initial parameters which are closer to true (refined) ones would not only assure faster and saver convergence, as result of the refinement procedure, but also allow the possibility that reached refined convergent set would be closer to the true values and ultimately increase the reconstruction accuracy [15]. Specifically, using orthogonal attached wands we show two common ways to provide linear constraints on a geometric entity known as the absolute conic. Hence, internal camera parameters are then in principle trivially obtainable.

2. Theoretical background

Our approach of extracting initials value of camera parameters starts with the identification of the image of the absolute conic (IAC). The complete description and properties of the absolute conic and its image can be found elsewhere [16]. Here, only the basics will be reviewed.

The absolute conic is a conic on the plane at infinity, consisting of points **X** such that

$$\begin{aligned} X &= [x \quad y \quad z \quad t] \quad t = 0 \\ x^2 + y^2 + z^2 &= 0 \end{aligned} \tag{1}$$

where points with t=0 are called points at infinity and their images are so called vanishing points **v**. Writing the first three components of point **X** separately as **d** the defining equation for the absolute conic within the plane at infinity, has even simpler form:

$$\begin{aligned} d &= [x \quad y \quad z]^T \\ d^T \cdot d &= 0 \end{aligned} \tag{2}$$

Let us recall the decomposition of a camera's projection matrix **P**,

$$P = K \cdot [R \mid -R \cdot t] \tag{3}$$

where **K** is the upper triangular matrix of internal camera parameters, **R** and **t** represent external camera parameters (orientation and position). The image point (i.e. vanishing point) corresponding to a point at infinity mapped by a camera with matrix **P** (3) is given by

$$v = P \cdot [d \quad 0]^T = K \cdot R \cdot d \tag{4}$$

Solving (4) for **d** and combining with (2) gives:

$$v^T \cdot (K \cdot K^T)^{-1} \cdot v = v^T \cdot \omega \cdot v \tag{5}$$

Image point **v** is on the image of the absolute conic if and only if (5) is equal to zero. Thus, the image of the absolute conic is a plane conic **ω** represented by the matrix $(\mathbf{K}\mathbf{K}^T)^{-1}$. Obviously, the internal camera parameters are neatly embedded in the IAC and once the matrix **ω** is found, its Cholesky decomposition would yield us the matrix **K** itself. It can further be shown that the angle α between two lines in 3D space can be found using the information about the vanishing points $\mathbf{v_1}$ and $\mathbf{v_2}$ of those two lines and **ω**:

$$\cos\alpha = \frac{v_1^T \cdot \omega \cdot v_2}{\sqrt{\left(v_1^T \cdot \omega \cdot v_1\right) \cdot \left(v_2^T \cdot \omega \cdot v_2\right)}} \tag{6}$$

Conversely, if the angle between two lines is known we have a constraint on **ω**. Generally, the above expression is quadratic. However, assuring that the angle between the lines is 90° will give us a linear constraint:

$$v_1^T \cdot \omega \cdot v_2 = 0 \tag{7}$$

The matrix **ω** is symmetric and defined up to scale. Without any further assumption about internal camera parameters (such as zero skew or known aspect ratio) we need a minimum of five such orthogonal line pairs to find a solution for **ω**. With more than five pairs a least squares solution can be found. And in our case during the wand dance with an orthogonal triad of wands this is exactly what is obtained. Vanishing points themselves can be commonly found as intersections of images of parallel lines or, as it is in our case, from known ratios on single lines.

A similar linear constraint to (7) can be acquired for any point whose image lies on the IAC. In the case of planar projective geometry we can define two characteristic points, so called circular points (or, absolute points). The circular points **I** and **J** are a pair of complex conjugate ideal points:

$$I = [1 \quad i \quad 0]^T \quad J = [1 \quad -i \quad 0]^T \qquad \textbf{(8)}$$

For a given plane, points at infinity all lie on the so-called line at infinity. The name 'circular points' originated from the fact that every circle intersects the line at infinity at the mentioned circular points. In 3D projective space every plane $\boldsymbol{\pi}$ intersects the plane at infinity $\boldsymbol{\pi}_\infty$ at the line at infinity $\mathbf{l}_\infty$ of that particular plane $\boldsymbol{\pi}$. Also, this line $\mathbf{l}_\infty$ intersects the absolute conic in two circular points of plane $\boldsymbol{\pi}$. Furthermore the images of those circular points lie on the IAC. Thus, if we can find the homography **H** between some plane $\boldsymbol{\pi}$ and the camera image plane we can easily apply that homography **H** on the circular points (8) to find images of circular points. Knowing the images of circular points we have another linear constraint on the elements of the IAC, similar to (7). Let $\mathbf{h_1}$ and $\mathbf{h_2}$ be the first two columns of **H**, then:

$$(h_1 \pm i \cdot h_2)^T \cdot \omega \cdot (h_1 \pm i \cdot h_2) = 0 \qquad \textbf{(9)}$$

This constraint on $\boldsymbol{\omega}$ is used also in [5], [6]. To find the plane homography **H** a minimum of four points are needed. In our case, each pair of orthogonal wands represents such a plane $\boldsymbol{\pi}$ and from markers on the wands, the homography **H** can thus be computed.

3. Materials and methods

The 3D reconstruction system used during the course of this work, called Smart, is commercially available by the eMotion company [13]. The system version used (version 1.10, Build 2.39) consists of 9 cameras (50 Hz). It is a so-called optoelectronic system which actually reconstructs positions of passive retro-reflective markers, attached to the subject's points of interest. Markers are illuminated by stroboscopic IR sources of light attached to the cameras and the cameras are additional equipped with IR filters. Smart is installed in the Biomechanic laboratory of Peharec Polyclinic in Pula, Croatia [17]. The system is there used on a daily basis for various motion analyses of healthy and injured subjects. For more in-depth motion analysis the synchronized system add-ons are also two Kistler force platforms and 8 channels EMG device.

The first experiment consisted of a typical system calibration as proposed by the system's manufacturer. An orthogonal triad (each axis 60cm long) was positioned on the floor (Figure 1). Each axis of the triad defined one of the world coordinate axes and had a certain number of retro-reflective markers on it. The vertical axis Y had 3 markers and the horizontal axes, X and Z, had 4 and 2, respectively. The relative positions of markers are accurately known. A visual check if each camera 'sees' all triad wands, i.e. the markers on it, was performed and the image acquisition was undertaken for a few seconds. Afterwards, as a part of the second step, the orthogonal triad was removed and a wand dance with a single wand was performed for a couple of minutes. The entire procedure was carried out by trained polyclinic personnel to ensure that calibration results would not be impaired by inexperience. Finally, Smart's software routines were started to compute cameras parameters based on acquired images from the above two calibration steps.

In the second experiment, our approach was used where the wand dance started right away with the orthogonal triad. It lasted roughly 60 seconds (half of the time proposed by Smart for its wand dance with a single wand) and at the end the triad was simply put on the floor to set the origin of the working volume's coordinate system. In both experiments, the volume was approximately 3.2m × 2.2m × 2.0m.

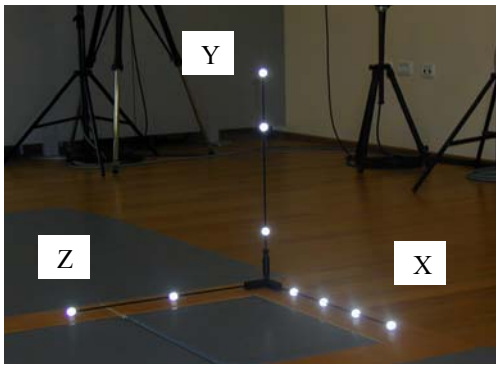

Figure 1. Image of the orthogonal triad with attached markers. Markers distances [cm] with respect to the triad origin are: X-axis 15, 30, 45, 60; Y-axis 15, 45, 60; Z-axis 30, 60.

4. Results

Besides a rather comprehensive analyzing software, Smart also has the capability to export/import various data into/from Matlab: 2D image data (extracted marker centroids for the acquired sequence), 3D reconstruction data for the markers, camera projection matrices etc. Three things were exported for further analysis: 2D image data of markers for the orthogonal triad when put to the floor which otherwise serves for camera parameter initialization in the Smart calibration procedure. Then, camera projection matrices calculated by Smart's calibration procedure were exported and finally the 2D image data corresponding to the wand dance with the orthogonal axes triad.

Once exported into Matlab the following was calculated. First, based on 2D image data of markers on the orthogonal triad and their known spatial relationship, camera projection matrices were calculated which are supposed to be further processed by the Smart software to refine them after the wand dance. Next, from 2D image data of the orthogonal triad wand dance, vanishing points for each axis were calculated in each frame, for all different cameras, using the known length ratios of the markers. As explained before this enabled us to set up

linear equations to compute the IAC and consequently an initial set of internal camera parameters. This type of calibration will be further referred to in the text as Type A. Finally, again from the wand dance and due to the known spatial configuration of some orthogonal wands and their markers (which define a plane), and along with their image coordinates, we computed plane homographies. These were used like described above to establish another set of linear constraints on the IAC. This type of calibration will be further referred to as Type B.

Initial values of internal camera parameters from the Smart method, final values as provided by Smart and from our two approaches (Type A and Type B) are given for comparison in Table 1, Table 2, Table 3 and Table 4, respectively. Each row represents values for one of the nine cameras. Once the internal parameters of cameras are known and given enough image correspondences for every camera pair, their fundamental matrix can be calculated and therefore the orientation of each camera with respect to each other can be extracted from [16]. Finally, the complete projection matrices for each camera pair can be constituted. Projection matrices originating from data in Table 1, Table 3 and Table 4 were separately calculated in order to reconstruct the length of the wand during the wand dance. Furthermore, the same length was reconstructed using the (final) projection matrices provided by Smart and exported in Matlab. Mean errors between reconstructed and true lengths (45cm) are given in Table 5 for all 36 possible camera pairs. The first, second, third and fourth columns reflect data from Table 1, final Smart provided projection matrices (Table 2), Table 3 and Table 4 respectively. All 3D reconstructions and length calculations are performed on distorted image coordinates and no distortion correction was undertaken.

Table 1.Internal camera parameters, initial values, Smart

Focal length [pixels]		Skew factor	Principal point [pixels]	
X direction	Y direction			
751,9	387,0	12,7	400,0	175,3
755,6	381,0	18,3	330,3	233,5
676,6	343,3	7,4	272,3	200,5
704,1	367,4	6,4	320,7	171,3
765,2	399,0	5,0	335,9	170,2
746,8	386,4	19,0	376,9	215,3
691,0	354,6	9,2	285,3	164,5
672,7	343,3	14,4	297,2	142,7
672,8	348,2	10,3	292,1	156,2

Table 2. Internal camera parameters, refined values, Smart

Focal length [pixels]		Skew factor	Principal point [pixels]	
X direction	Y direction			
727,7	375,9	0,0	349,4	153,7
723,8	374,6	0,0	304,4	145,4
723,9	375,2	0,0	290,3	138,4
724,3	374,7	0,0	325,4	140,0
724,2	375,1	0,0	347,7	137,0
724,8	375,0	0,0	349,9	143,4
719,2	371,8	0,0	328,9	134,7
730,1	377,2	0,0	350,7	133,4
715,9	370,5	0,0	345,0	138,6

Table 3. Internal camera parameters, initial values, our first approach (type A)

Focal length [pixels]		Skew factor	Principal point [pixels]	
X direction	Y direction			
724,8	376,2	0,0	376,9	128,0
749,7	390,0	0,7	321,9	136,0
743,4	390,7	-0,5	267,5	132,1
728,3	376,5	-0,3	346,9	133,5
715,6	373,8	-1,5	332,8	145,2
734,6	381,0	0,2	381,5	136,6
715,3	372,9	-2,3	274,4	126,3
704,4	370,2	0,9	308,0	122,2
723,3	373,4	0,5	341,9	136,2

Table 4. Internal camera parameters, initial values, our second approach (type B)

Focal length [pixels]		Skew factor	Principal point [pixels]	
X direction	Y direction			
683.91	354.36	0	379.76	128.79
689.64	357.33	0	322.63	135.05
669.16	346.71	0	260.05	138.78
699.19	362.27	0	343.82	138.23
695.17	360.19	0	368.39	141
709.06	367.39	0	391.62	140.19
640.2	331.71	0	312.66	172.37
688.78	356.88	0	362.46	131.42
676.49	350.52	0	357.15	143.89

Table 5. Mean length error between reconstructed and true wand length [mm]

Smart initial	Smart final	Proposed method, type A	Proposed method, type B
22.84	8.82	15.09	11.85
16.00	8.21	7.66	7.56
15.16	6.91	4.52	9.29
13.01	6.18	3.95	7.88
22.98	9.01	6.99	6.74
13.15	11.48	3.60	14.57
13.92	5.42	5.05	8.61
11.93	7.15	3.98	7.68
19.37	6.35	6.87	8.45
17.06	5.73	4.98	7.18
15.24	5.14	4.12	7.14
24.92	7.18	9.66	7.30
15.18	8.49	5.40	16.56
15.54	4.69	5.65	7.78
30.62	6.07	4.96	7.32
15.13	5.82	4.52	6.41
38.16	10.86	6.58	9.06
23.22	7.41	6.03	5.71
15.59	10.27	14.41	61.37
14.46	4.74	5.29	10.08
12.03	4.82	3.78	8.01
14.16	5.47	6.30	7.08
23.99	6.72	6.20	10.01
14.38	6.52	3.86	15.81
15.48	5.93	6.18	7.62
10.88	4.86	3.96	8.51
20.73	6.06	4.58	7.75
15.94	9.48	4.11	14.01
13.24	5.32	7.15	8.50
7.85	4.59	6.05	11.93
21.50	10.93	4.55	10.84
21.62	6.89	6.33	9.32
18.48	5.13	4.69	7.91
12.55	7.22	5.66	13.01
8.90	6.43	2.87	10.32
13.14	5.04	13.85	8.73

5. Discussion and concluding remarks

The camera parameters in Table 2 are the result of Smart's refinement procedure. Although these values may still not be the perfect true ones they can at least be regarded as very close to the true ones. Thus, an initialization that gives closer values to these refined ones is generally more desirable. A closer comparison of Table 1 (initial values by Smart) and Table 3 (initial values by type A) with Table 2 (Smart refined values) reveals that in practically all cases the parameters computed by type A calibration are quite closer to Smart's refined ones. The results obtained from type B calibration (Table 4) are not as good as type A, but still better than Smart's initial ones. The most likely reason for type A being better then type B has to do with the implementation (practical) issues.

Type B assumes the computation of planar homographies **H** between planes in space defined by two orthogonal wands and the image plane. To determine **H** we need a minimum of four point correspondences. In the presence of noise the computed **H** would be more accurate if one had more than four correspondences and hopefully equally distributed throughout the plane. However, in our case equal distribution is not possible since we are obtaining correspondences from markers attached on two orthogonal wands forming the plane. Consequently, images of circular points, found by such **H,** will not provide optimal constraints for the linear equation system used to compute the IAC. An additional practical issue with type B calibration, noticed throughout experimentation, is to avoid frames where images of two wands make small angles. Including such images, together with noise, would impair the ultimate solution for camera parameters. We set a rather strict threshold value which discards all those frames where the angle between wands in the image plane is less than 80º. This threshold left us with even less data (redundancy) for subsequent processing. One feature that brought an improvement for type B was enforcing the zero skew and known aspect ratio. Given the fact of working with high quality cameras those two assumptions are reasonable. First, a so-called soft constraining was tried to enforce the mentioned values. It basically means adding a couple of more equations to the equation system, where appropriate elements of IAC are explicitly set to zero, i.e. to a known ratio. As intuitively expected, the significance of adding those two equations to a system of a large number of equations (~several thousands) was negligible. Second, a so called hard constraining was undertaken. In this case the system of equations to calculate elements of IAC was set right from the start to accommodate the fact of zero skew and known aspect ratio (thus, decreasing the number of unknowns in the IAC). This approach did bring an improvement (not shown due to limited space) over the case where skew factor and both focal lengths were explicitly calculated as well. One can note that skew factors in Table 4 are all zero.

There are some noteworthy implementation issues for type A also. First at all, here the desired equal distribution of image points for calibration is easier to achieve. However, in this case two potentially problematic situations exist: wand positions which are (close to) either perpendicular or parallel to the image plane. The first problem is easily solved by discarding all those frames where the image distance between markers on a wand is less than a certain number of pixels. The second potential problem (parallelism) could have been resolved perhaps by detecting vanishing points that are at a large distance from the image center. However, we took a

different approach here. We start with considering vanishing points around the image center and then gradually increasing the image area, taking more and more vanishing points into the computation of the IAC. Each time a different set of vanishing points would give us different set of camera parameters. How to choose the right set? We accept the set which has the smallest skew factor. Namely, vanishing points which originated from those wand positions close to parallel with the image plane and under the influence of noise will be quite off their true values. Consequently, including such data, and perhaps some others that are also for some reason quite off, will very likely give incorrect values for internal camera parameters. One parameter that we know for a fact value is the skew being zero. Thus, it is reasonable to accept that set of IAC elements that contains the smallest skew is the one satisfactory approaching true parameter values. Analyzing type A and type B we can conclude that type A calibration would be the method of choice for parameter initialization.

To test the quality of initial sets of parameters, perhaps the simplest, 3D reconstruction was undertaken, assuming a linear camera model and no distortion correction. Furthermore, testing separate camera pairs gave insight of results consistency for various camera configuration setups. As shown in Table 5, the mean errors of our two approaches are not only significantly better than when using Smart's initial results, but results from type A are in particular very close to the case when final Smart's parameter sets are used. That strongly indicates, once again, that our initial set is very close to Smart's final one.

It has already been noted that closeness of the initial solution to the final one highly determines speed of convergence and in a large number of cases determines whether there will be any convergence or none at all. It is not rare in practice that after Smart parameters refinement is done the user is notified that calibration failed due to the fact that no convergent set of solutions is obtained and the calibration procedure has to be done again. Or giving the larger residuals of parameter refinement procedure the user is indirectly encouraged to redo calibration anyway. That is another issue that goes in favor of our approach which gives as initial estimates values closer to the final ones and when starting with them it is less likely that the calibration procedure will have to be repeated.

Let us underline that Smart's final sets of parameters are used also on distorted image data, using the linear camera model. For completeness, we need to say that the 3D reconstruction mean errors that Smart normally outputs, *after* distortion correction on images, are of the order of millimeter, in the case where camera pairs are considered. In case where all available cameras are simultaneously used for triangulation, results are even better. The exact procedure how Smart refines parameters, based on known wand length, is not known to the authors. Besides, an open question still remains what would be our wand length reconstruction results after parameter refinement, either for type A or for type B. The answer to that question is left for future work. Still, closeness of our initial sets of solution to Smart's final ones strongly suggests that it should be at least about the same, if not perhaps better.

References

[1] http://www.simple3d.com/
[2] P. Allard, I. Stokes and J.-P. Blanchi. Three Dimensional Analysis of Human Movement. Human Kinetics, Champaign, 1995.
[3] K.B. Atkinson. Close Range Photogrammetry and Machine Vision. Whittles Publishing, 1996.
[4] G.Q. Wei and S.D. Ma. Implicit and explicit camera calibration: theory and experiment. IEEE Trans. Pattern Analysis and Machine Intelligence, 16(5), 469-480, 1994.
[5] Z. Zhang. A flexible new technique for camera calibration. IEEE Transactions on Pattern Analysis and Machine Intelligence, 22(11), 1330-1334, 2000.
[6] P. Sturm and S. Maybank. On Plane-Based Camera Calibration: A General Algorithm, Singularities, Applications, IEEE Conference on Computer Vision and Pattern Recognition, 432-437, 1999.
[7] N.A. Borghese and P. Cerveri. Calibrating a video camera pair with a rigid bar. Pattern Recognition, 33, 81-95, 2000.
[8] R. Hartley. Kruppa's equations derived from the fundamental matrix. IEEE Transactions on Pattern Analysis and Machine Intelligence, 19(2), 133-135, 1997.
[9] B. Caprile and V. Torre. Using Vanishing Points for Camera Calibration, International Journal of Computer Vision, 4, 127-140, 1990.
[10] D. Liebowitz and A. Zisserman. Metric rectification for perspective images of planes. IEEE Conference on Computer Vision and Pattern Recognition, 482-488, 1998.
[11] R. Hartley, L. de Agapito, E. Hayman and I. Reid. Camera calibration and the search for infinity. IEEE Int. Conference on Computer Vision, 510-517, 1999.
[12] P. Sturm. Critical motion sequences for the self calibration of cameras and stereo systems with variable focal length. Image and Vision Computing, 20(5-6), 415-426, 2002.
[13] eMotion/Smart http://www.emotion3d.com, Vicon Motion Systems. http://www.metrics.co.uk/, BTS/Elite http://www.bts.it/en/index.html
[14] H. Hatze. High-precision three-dimensional photogrammetric calibration and object space reconstruction using a modified DLT approach. J. Biomech., 21, 533-538, 1988.
[15] W.H. Press, S.A. Teukolsky, W.T. Vetterling and B.P. Flannery, Numerical Recipes in C. Cambridge University Press, 1997.
[16] R. Hartley and A. Zisserman, Multiple View Geometry in Computer Vision, Cambridge University Press, 2000.
[17] http://www.peharec.com/index.html